Fibre bragg grating based attitude sensor

Fibre Bragg Grating based Attitude Sensor

Nikolitsa Papachristou, Jonathan Morton, Adrian Dzipalski, Dimitrios Polyzos, Robert R. J. Maier, William N. MacPherson

Institute of Photonics and Quantum Sciences, School of Engineering and Physical Sciences, Heriot-Watt University, Edinburgh, UK
Author e-mail address: np15@hw.ac.uk

Abstract: We present a system of three Fibre Bragg Grating (FBG) curvature sensors configured as a multi-axis attitude sensor. The FBG response on each sensor provides information about its deflection due to gravity acting on a sensing mass. The three sensor system can be processed to give 3-D attitude information with an accuracy of ±2° demonstrated. The fabrication, calibration and performance of the sensors is discussed.
OCIS codes: 060.2370 Fiber optics sensors, 060.3735 Fiber Bragg gratings

1. Introduction

Optical techniques have been reported extensively for attitude and directional bearing measurement, with the optical Gyroscope the most developed. Gyroscopes are well established and are important for inertial navigation systems where gyrocompasses are used on aircraft, space craft and ships [1]. The first optical gyroscope, the Ring Laser Gyroscope, was demonstrated by W. M. Macek and D.T. Davis in 1963 [2]. In 1976, V. Vali and R. W. Shorthill introduced the concept of the first Fibre Optic Gyroscope (FOG) [3], and since then other FOG configurations have been presented [1]. All configurations of FOGs exploit the same operating principle; the Sagnac effect [4].

Recent studies on FOGs, have focused on the improvement of their stability, with the interferometric fibre optic gyroscopes (IFOGs) reported to have negligible bias instability. One characteristic example is the IFOG fabricated by Qiang Yu, *et al.* in 2009 with stability of 0.001°/h [5]. There are several environmental parameters that introduce errors or drift on the performance of the FOGs: the gyroscope's environmental temperature, environmental magnetic fields and vibrations [6]. Additionally, the stability and coherence of the light source and polarization changes of the interfering beams needs to be considered when assessing the FOG's overall stability and performance [7].

Here we demonstrate a Fibre Bragg Grating (FBG) based sensor capable of providing information on the attitude of a given platform. Three FBG based curvature sensors are used in order to determine the angular alignment of the platform in three directions with respect to gravity. The FBG curvature sensors are essentially end mass-loaded cantilevers where the differential strain across their width can be determined using FBG strain gauges. Each sensor consists of four FBGs, however only three of them are necessary to determine curvature. The additional FBG on each sensor is used in order to form a square cross-section structure. This concept has already been reported in literature [8, 9] however here we explore the use of several sensing elements to extend the operating range of the overall system. In the intended application of this attitude senor the design is motivated by the need to determine the orientation of a subsea structure. This structure would include several other sensors which are compatible with the FBG technology used in the attitude sensor described here.

2. Sensors fabrication

The three FBG curvature sensors (C1, C2, and C3) were fabricated using the set up shown in figure 1 (left). For each sensor, four single mode fibres (SMFs) containing FBGs were used. The SMFs were positioned in a square alignment using specially designed holders and a longitudinal tension of 0.75 N was applied in order to maintain alignment. All FBGs were positioned at the same point along the sensor. An optical adhesive (Norland 68) was used in order to glue the four fibres together: a controlled volume of adhesive was applied along the fibres using an automated syringe pump. Directly after the adhesive implementation, a ring of UV LEDs (375 nm) passed along the fibres, thus the adhesive could be cured uniformly. Several passes of the UV LED curing ring ensured complete curing of the adhesive and stabilized the structure rigidity of the sensor. Figure 1 (middle and right) shows a cross section of the four SMFs (square structure) after the adhesive has cured.

The FBGs 'stem' was fixed on a plastic base thereby forming a simple cantilever (figure 2(a)). According to beam theory the maximum deflection of a cantilever depends on the applied force, the length, and the material properties of the cantilever. In this case the force is due to the Earth's gravity acting upon a small mass of around 1.30 grammes attached to the sensor stem. The total length of the FBGs is 1 cm and the stem was held 6 mm below the centre of the FBGs as illustrated in figure 2(b).

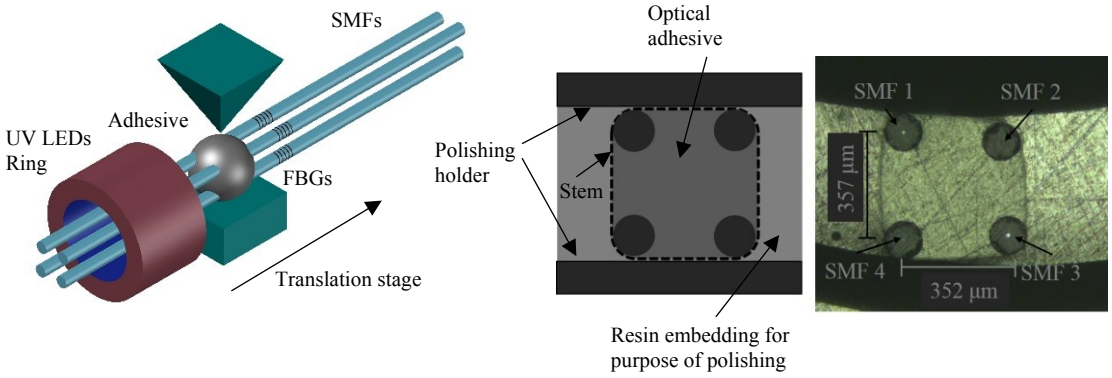

Figure 1. (left) FBG curvature sensors fabrication set up, (middle) Schematic cross section of the FBG curvature sensor (right), image of the cross from a microscope with illuminated cores of SMF1 and SMF3 (right).

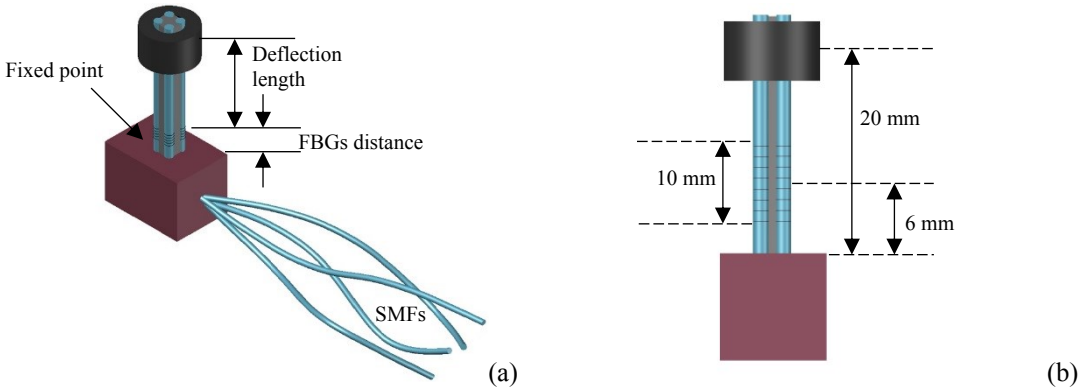

Figure 2. FBG curvature sensor used on the attitude sensor (a) 3-D view, (b) 2-D view.

3. Sensor Calibration

According to beam theory the curvature, κ, at distance, z, from the fixed end can be calculated using the equation [8]:

$$\frac{1}{R} = \kappa = \frac{3(l-z)}{l^3} d \quad (1)$$

where, l is the length of the cantilever, d is the deflection at the loading point, and R is the curvature raduis.

The wavelength shift of the Bragg grating inscribed in the fibre is proportional to the strain applied to the structure. Suitable linear calibration can be achieved by deflecting the sensor in two orthogonal directions by known amounts and measuring the change in reflection wavelength as shown in figure 3(a). The wavelength difference between two pairs of FBGs has a linear relationship with the curvature of the sensor at the two directions:

$$\Delta\lambda_{12} = c_{12} + p\kappa_1 + q\kappa_2 \quad (2)$$
$$\Delta\lambda_{23} = c_{23} + r\kappa_1 + s\kappa_2 \quad (3)$$

where κ_1 and κ_2, is the curvature of the sensor in the two directions and can be calculated through equation 1 for any amount of deflection, by setting z to the distance of the centre of the FBGs from the fixed end point (6 mm). The calibration parameters, $c_{12}, c_{23}, p, q, r, s$ can be extracted from the linear fittings of the corresponding graphs.

Figure 3(b) shows the reflected wavelength for one FBG upon deflection. The sensor end was deflected in 0.5 mm increments and the FBG peak wavelengths were monitored for 60 seconds (total sensor deflection 2.5 mm). For the given deflection the FBG was stretched (on the outer side of the curve) thus the wavelength of the peak reflectivity increased. The response of all four gratings was monitored simultaneously. The same procedure was repeated for the second direction of deflection (i.e. applying the deflection at 90° with respect to the first tests). The calibration parameters were extracted from the wavelength responses of the FBGs 1, 2 and 4. Figures 4(a) and (b) show the linear fittings of the FBGs wavelength shifts over the curvature of the sensors for the two directions. The linear calibration was applied to all three FBG curvature sensors forming the attitude sensor.

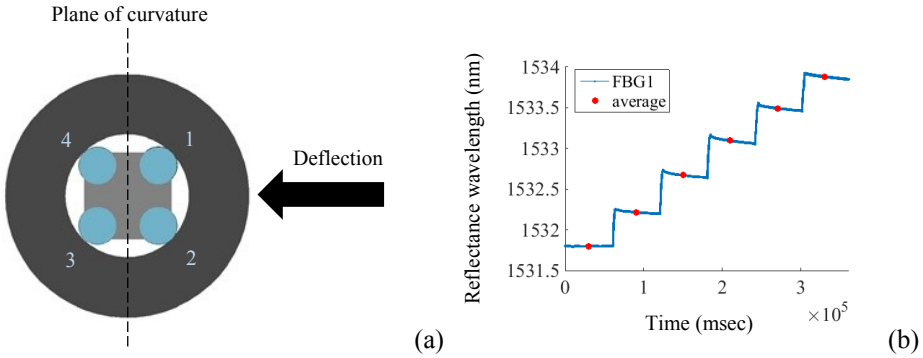

Figure 3. (a) Sensor cross-section showing core orientation and deflection direction. (b) Reflection spectra for FBG1 upon linear deflection

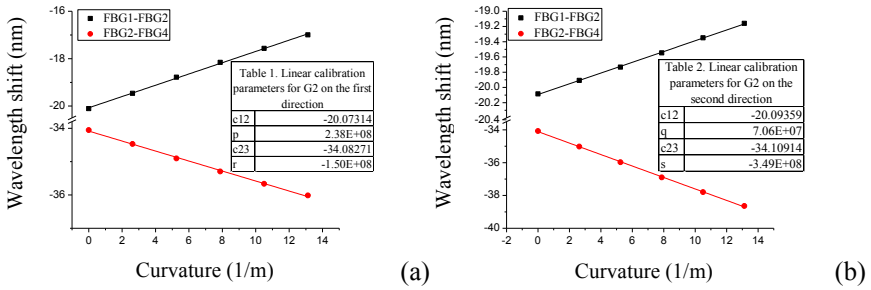

Figure 4. Wavelength shift of the FBGs pairs over the sensor's curvature and linear calibration parameters on directions (a) as shown in figure 3(a) and (b) 90° with respect to the first.

4. Rotational calibration of the sensors

The rotational calibration was performed by rotating each sensor through 360° in the same two directions used in the calibration above. The first direction is shown schematically in figure 5(a). The peak wavelength response from all FBGs upon rotational deflection, was monitored for 30 seconds with 10° step rotation of the sensor. Figure 5(b) shows the response of FBG1 on the first rotational direction.

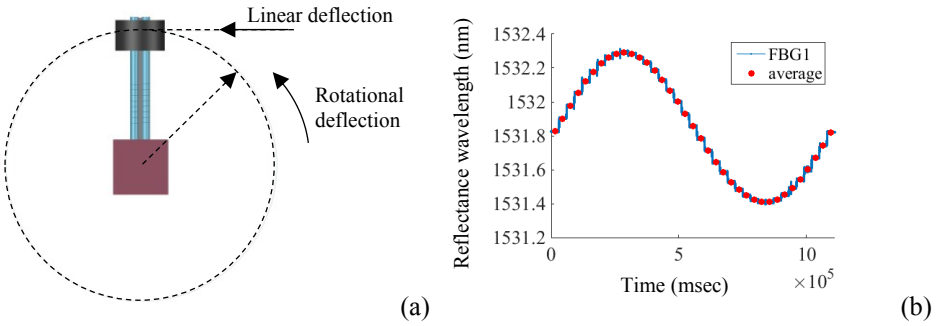

Figure 5. (a) Direction of the first rotational deflection of the sensor, (b) Reflectance wavelength response of FBG1 upon rotation

According to equations 1, 2 and 3 the curvature of the sensor at the loading point on the two directions (d_1, d_2) can be calculated by monitoring the wavelength peak positions of the FBGs:

$$\kappa_1 = \frac{s}{sp-qr}(\Delta\lambda_{12} - c_{12}) - \frac{q}{sp-qr}(\Delta\lambda_{23} - c_{23}) = \frac{3(l-z)}{l^3}d_1 \quad (4)$$

$$\kappa_2 = \frac{p}{sp-qr}(\Delta\lambda_{23} - c_{23}) - \frac{r}{sp-qr}(\Delta\lambda_{12} - c_{12}) = \frac{3(l-z)}{l^3}d_2 \quad (5)$$

Figures 6(a) and (b) show the deflection of the sensor as a function of its rotational alignment. The maximum deflection, and therefore the highest peak wavelength difference, occurs at 90° and 270° positions. A sinusoidal fitting on the experimental data can provide the angular deflection of the sensor in each direction. Thus, by monitoring the FBG peak wavelengths of the curvature sensor, the angular deflections (φ_1 or φ_2) on the two directions of the sensor can be extracted from the following equation:

$$\varphi_{1/2} = \frac{w}{\pi}\sin^{-1}\frac{(d_{1/2} - d_0)}{A} + c \quad (6)$$

where, d_1 and d_2, can be calculated from equations 4 and 5. Moreover, w and A are the period and the amplitude extracted from the sinusoidal fitting respectively. Finally, d_0 and c are displacement constants provided from the fitting data. All parameters for the two directions of deflection for C2 sensor that are provided from the fitted data are included in figure 6(a) and (b).

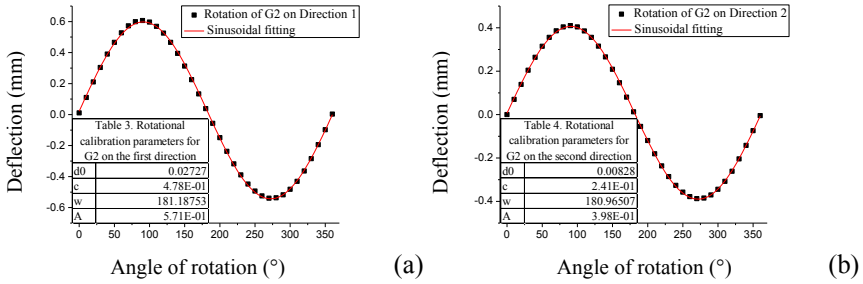

Figure 6. Rotational deflection of the C2 sensor on the two directions (a) as shown in figure 5(a) and (b) 90° with respect to the first one.

5. The complete attitude sensor

The final arrangement of the gyroscope is shown in figure 7. The three FBG curvature sensors are fixed on three positions perpendicular to each other (on x, y and z axis), three wavelength division multiplexers (WDMs) were used to monitor all the FBGs spectra from the three sensors. The first and the second sensors (C1 and C2) provide information about the rotation on xz – plane and yz –plane respectively. Finally, the third sensor (C3), is used to determine the upright position of the gyroscope. Each sensor can provide reliable information about the rotation of this configuration within the range of 180° in one plane. When this sensor exceeds this range, information about the orientation in this plane can be provided by the next orthogonal sensor. The signal noise on the calibration curves is an average of 0.03 nm. Therefore this configuration can be used for gyroscope measurement applications with accuracy of ±2°.

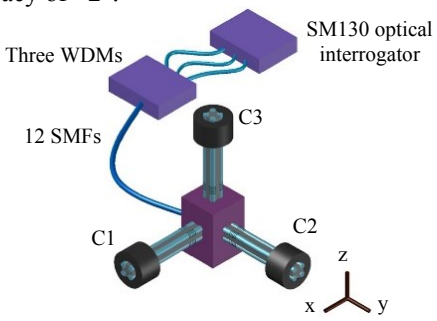

Figure 7. Schematic illustration of the final arrangement of the gyroscope.

6. Conclusions

We report the fabrication and use of three FBG based curvature sensors as a means of determining the attitude of a system platform with sensitivity of ±2°. Weights attached on each sensor induce deflection due to orientation, which can be determined by monitoring the peak wavelength shift of the FBGs.

7. Acknowledgements

The authors would like to acknowledge funding from the European Union's Horizon 2020 research and innovation programme under grant agreement No 635568: LAkHsMI Project.

8. References

[1] V. M. N. Passaro, A. Cuccovillo, L. Vaiani, M. Carlo, and C. E. Campanella, "Gyroscope Technology and Applications: A Review in the Industrial Perspective," *Sensors (Basel),* vol. 17, no. 10, (2017).
[2] W. M. Macek and D. T. M. Davis, "Rotation Rate Sensing with Traveling-Wave Ring Lasers," *Applied Physics Letters,* vol. 2, no. 3, pp. 67-68, (1963).
[3] V. Vali and R. W. Shorthill, "Fiber ring interferometer," *Applied Optics,* vol. 15, no. 5, pp. 1099-100,(1976).
[4] H. J. Arditty and H. C. Lefèvre, "Sagnac effect in fiber gyroscopes," *Optics Letters,* vol. 6, no. 8, p. 401, (1981).
[5] Y. Qiang, L. Xuyou, and Z. Guangtao, "A kind of hybrid optical structure IFOG," pp. 5030-5034, (2009).
[6] K. Böhm, K. Petermann, and E. Weidel, "Sensitivity of a fiber-optic gyroscope to environmental magnetic fields," *Optics Letters,* vol. 7, no. 4, p. 180, (1982).
[7] E. C. Kintner, "Polarization control in optical-fiber gyroscopes," *Optics Letters,* vol. 6, no. 3, p. 154, (1981).
[8] G. M. H. Flockhart, W. N. MacPherson, J. S. Barton, and J. D. C. Jones, "Two-axis bend measurement with Bragg gratings in multicore optical fiber," *Optics Letters,* vol. 28, no. 6, p. 3, (2003).
[9] B. J. Wolf, J. A. S. Morton, W. B. N. MacPherson, and S. M. van Netten, "Bio-inspired all-optical artificial neuromast for 2D flow sensing," *Bioinspiration and Biomimetics,*(2018).